# Microscopic theory for the influence of Coulomb correlations in the light-emission properties of semiconductor quantum wells

M. F. Pereira, Jr. and K. Henneberger
*Fachbereich Physik, Universität Rostock, D-18051 Rostock, Germany*
(Received 20 February 1998)

A nonequilibrium Green's-function $T$-matrix approach is presented for the consistent computation of semiconductor quantum-well optical spectra including strong Coulomb correlations in the coupled photon and carrier system. Numerical solutions of the Bethe-Salpeter-type equations yield good agreement with recent absorption and/or gain and emission experiments. [S0163-1829(98)02428-X]

## I. INTRODUCTION

The electronic properties of semiconductors are well understood in terms of many-body effects.[1] However, there is as yet no first-principles theory capable of realistically predicting the influence of Coulomb correlations in the evolution of light emission spectra of semiconductors with increasing carrier density consistently including, e.g., quasi-two-dimensional confinement and coupled band-structure effects, specially under incoherent excitation or cases in which the polarization is destroyed by fast dephasing processes within the detection time. To our knowledge, the first attempt to compute both multiple-quantum-well (MQW) absorption and luminescence spectra in a wide density range, including the light and carrier field operators on the same fully quantum-mechanical footing, has been given in Ref. 2. The general theory is formally sound and merits consideration for the interesting limiting cases it provides. However, the numerical applications presented are restricted to idealized conditions that give rise to serious shortcomings. The valence bands are parabolic and the Coulomb potential strictly two-dimensional. Dephasing effects that broaden the spectral lines are not included. The line shapes are not realistic, and the predicted emitted output reduces with increasing carrier density, in contrast to vast experimental evidence. The last limitation has been recently overcome by means of a broader spectral representation.[3] However, the idealized model with a bare Coulomb potential and parabolic bands is meaningful for quantum wires, as demonstrated by a good agreement with experimental data, but not for MQW's.[4,5] Altogether, the approximations cannot realistically describe MQW absorption and/or gain and emission spectra.[4,5] Finally, in both Refs. 2 and 3 and previous work in the literature, the equations do not present a consistent way to include higher order Coulomb correlations in all relevant self-energies, and thus do not provide the means to check their importance by means of optical experiments. In this paper, MQW absorption and/or gain and light emission are consistently modeled and the numerical results are in good agreement with steady-state experiments. The technique is able to describe the evolution from purely excitonic systems at very low density to the highly excited, inverted medium regime, where a plasma of interacting electron holes dominates the spectra. Low and/or high energy side artifacts in the gain and/or luminescence are eliminated in our approach by ensuring that the polarization function satisfies the Kubo-Martin-Schwinger (KMS) condition.[1,6] The paper is organized as follows. In Sec. II we summarize the main steps in the derivation of the Green's-function equations. We start with the Hamiltonian and necessary definitions and present a step by step derivation of the Bethe-Salpeter-type equations using functional derivative techniques. Equations for coupled multisubband quantum-well systems are derived in Sec. III. Numerical results and discussions are presented in Sec. IV, which is followed by a brief summary. Complementary results, which we refer to in the main text, are summarized in the Appendixes, including a derivation of the $T$-matrix equation in the electron-hole case and its relation to the correlation self-energy.

## II. NONEQUILIBRIUM GREEN'S-FUNCTION EXPRESSIONS

In this section, we summarize the main steps in the derivation of the Green's-function expressions, which are valid under nonequilibrium conditions and give rise to a quantum statistical description of light-emission and absorption processes in semiconductors including higher-order Coulomb correlations. A few of the equations, such as the starting point Hamiltonian, have been presented in a previous publication,[7] but are repeated here under a different notation, with band indices explicitly written. This alternative presentation is necessary to clarify some of the functional derivative steps, notably those involving the polarization function and the $T$-matrix equations given in the Appendix.

### A. Hamiltonian and Dyson equations

The laser-excited semiconductor is described by means of a many-particle Hamiltonian, which can be separated in electronic (el), electron-light-field interaction ($I$), free-field ($F$) terms,[8]

$$H = H_{\mathrm{el}} + H_I + H_F , \tag{1a}$$

$$H_{\mathrm{el}} = \sum_a \int \Psi_a^\dagger(\vec{R}) H_0 \Psi_a(\vec{R}) d\vec{R} + \frac{e^2}{2} \sum_{a,b} \int \Psi_a^\dagger(\vec{R}) \Psi_b^\dagger(\vec{R}') V(\vec{R}-\vec{R}') \times \Psi(\vec{R}')_b \Psi_a(\vec{R}) d\vec{R} d\vec{R}' , \tag{1b}$$

 

$$H_I = -\frac{e}{cm_0}\sum_{a,b}\int \Psi_a^\dagger(\vec{R})\vec{p}\cdot\vec{A}(\vec{R})\Psi_b(\vec{R})d\vec{R}$$

$$= -\frac{1}{c}\sum_{a,b}\int \vec{J}_{ab}(\vec{R})\cdot\vec{A}(\vec{R})d\vec{R}, \tag{1c}$$

$$H_F = \sum_{\lambda,\vec{q}} \hbar\omega_q(d^\dagger_{\lambda,\vec{q}}d_{\lambda,\vec{q}} + 1/2), \tag{1d}$$

where the labels $a,b,c,\ldots$ denote generically the several conduction and valence subbands, $\Psi(\vec{R})$ denotes the electron field operator, and $V(\vec{R}-\vec{R}') = e^2/\epsilon_0|\vec{R}-\vec{R}'|$ is the instantaneous bare Coulomb interaction. The current density operator reads

$$\vec{J}_{ab}(\vec{R}) = \frac{-ie\hbar}{2m_0}\{\Psi_a^\dagger(\vec{R})\nabla\Psi_b(\vec{R}) - [\nabla\Psi_a^\dagger(\vec{R})]\Psi_b(\vec{R})\}. \tag{2}$$

The vector potential operator $\vec{A}$ is expanded in terms of creation ($d^\dagger_{\lambda\vec{q}}$) and annihilation operators ($d_{\lambda,\vec{q}}$) of photons in the Coulomb gauge. In order to derive a hierarchy of equations valid for both equilibrium and nonequilibrium conditions, we consider the action of external charges $\rho_{\rm ext}$ and currents $\vec{J}_{\rm ext}$, and we describe the effect through the addition of an external term to the total Hamiltonian,

$$H_T = H + H_{\rm ext}, \tag{3a}$$

$$H_{\rm ext} = \int [\rho_{\rm ext}(\vec{R},t)\Phi(\vec{R}) - 1/c\vec{J}_{\rm ext}(\vec{R},t)\cdot\vec{A}(\vec{R})]d\vec{R}. \tag{3b}$$

The scalar potential $\Phi(\vec{R})$ is the solution of Poisson's equation,[8,7]

$$\Phi(\vec{R}) = \int \rho_{\rm tot}(\vec{R}')V(|\vec{R}-\vec{R}'|)d\vec{R}', \tag{4}$$

where we have introduced the total charged particle density, $\rho_{\rm tot} = \rho + \rho_{\rm ext}$, and

$$\rho(\vec{R}) = \sum_a \rho_a(\vec{R}) = e\sum_a \Psi_a^\dagger(\vec{R})\Psi_a(\vec{R}). \tag{5}$$

The excited semiconductor is described by nonequilibrium Green's functions for the interacting quasiparticles: carriers ($G$), photons ($D$), and plasmons ($W$), by

$$i\hbar G_{ab}(\underline{1}\,\underline{2}) = \langle\Psi_a(\underline{1})\Psi_b^\dagger(\underline{2})\rangle, \tag{6a}$$

$$\vec{D}(\underline{1}\,\underline{2}) = -\frac{c}{4\pi}\frac{\delta\vec{A}_{\rm eff}(\underline{1})}{\delta\vec{J}_{\rm ext}(\underline{2})},$$

$$W(\underline{1}\,\underline{2}) = \frac{\delta\Phi_{\rm eff}(\underline{1})}{\delta\rho_{\rm ext}(\underline{2})}, \tag{6b}$$

where we have used functional derivatives with respect to the external perturbations. The quantum-mechanical averages are calculated along the double-time Keldysh contour, $C$.[9] Time arguments running along $C$ are underlined, and $T_C$ denotes the time-ordering operator along $C$. In other words, the notation $\underline{1} = \vec{R}_1, t_1$ means that time runs under the contour from $-\bar{\infty}$ to $+\bar{\infty}$ on a positive branch, $\underline{t}_1 = t_+$ and back on a negative branch from $+\infty$ to $-\infty$, and thus $\underline{t}_1 = t_-$, e.g.,

$$\vec{A}_{\rm eff}(\underline{1}) = \langle\vec{A}(\vec{R}_1,\underline{t}_1)\rangle = \frac{{\rm tr}\{\rho_0 T_C[\vec{A}(\vec{R}_1,\underline{t}_1)S_C]\}}{{\rm tr}\{\rho_0 S_C\}}, \tag{7a}$$

$$S_C = T_C\ \exp\left(-i\int_C H_{\rm ext}(\underline{t})d\underline{t}\right). \tag{7b}$$

The Keldysh Green's-function time evolution is described by Dyson equations (sum over repeated arguments is assumed)

$$[G^{-1}_{0,ac}(\underline{1}\,\underline{3}) - \Sigma_{ac}(\underline{1}\,\underline{3})]G_{cb}(\underline{3}\,\underline{2}) = \delta_{ab}(\underline{1}\,\underline{2}), \tag{8a}$$

$$[\vec{D}_0^{-1}(\underline{1}\,\underline{3}) - \vec{P}(\underline{1}\,\underline{3})]\vec{D}(\underline{3}\,\underline{2}) = \vec{\delta}(\underline{1}\,\underline{2}), \tag{8b}$$

$$[W_0^{-1}(\underline{1}\,\underline{3}) - p(\underline{1}\,\underline{3})]W(\underline{3}\,\underline{2}) = \delta(\underline{1}\,\underline{2}), \tag{8c}$$

or equivalently,

$$\vec{D}(\underline{1}\,\underline{2}) = \vec{D}_0(\underline{1}\,\underline{2}) + \vec{D}_0(\underline{1}\,\underline{4})\vec{P}(\underline{4}\,\underline{3})\vec{D}(\underline{3}\,\underline{2}), \tag{9a}$$

$$G_{ab}(\underline{1}\,\underline{2}) = G_{0,ab}(\underline{1}\,\underline{2}) + G_{o,ac}(\underline{1}\,\underline{4})\Sigma_{cd}(\underline{4}\,\underline{3})G_{db}(\underline{3}\,\underline{2}), \tag{9b}$$

$$W(\underline{1}\,\underline{2}) = V(\underline{1}\,\underline{2}) + V(\underline{1}\,\underline{4})p(\underline{43})W(\underline{3}\,\underline{2}), \tag{9c}$$

where $\vec{\delta}$ is the transverse delta function. The bare Coulomb potential is diagonal in the time indices, $V(\underline{1}\,\underline{2}) = 1/|\vec{R}_1 - \vec{R}_2|\,\delta(t_1 - t_2)$. The inverse free propagators $G_0^{-1}$, $\vec{D}_0^{-1}$, $W_0^{-1}$, are given by

$$G^{-1}_{0,ab}(\underline{1}\,\underline{2}) = \left[i\hbar\frac{\partial}{\partial\underline{t}_1} - h_{\rm eff}(\underline{1})\right]\delta(\underline{1}\,\underline{2}), \tag{10a}$$

$$W_0^{-1}(\underline{1}\,\underline{2}) = -\frac{\epsilon_0}{4\pi e^2}\triangle_1\delta(\underline{1}\,\underline{2}), \tag{10b}$$

$$D_0^{-1}(\underline{1}\,\underline{2}) = [\triangle_1 - 1/c^2\partial^2/\partial\underline{t}_1^2]\delta(\underline{1}\,\underline{2}). \tag{10c}$$

Here, $\epsilon_0$ is the static dielectric function. The effective one-particle Hamiltonian in the equation for the free carrier propagator reads,

$$h_{\rm eff}(\underline{1}) = [H_0(\underline{1}) + \Phi_{\rm eff}(\underline{1})]\delta_{ab} + \frac{ei\hbar}{cm_0}\vec{A}_{\rm eff}(\underline{1})\cdot\nabla(\underline{1}). \tag{11}$$

The self-energies $\Sigma$, $\vec{P}$, and $p$ denoting, respectively, the carrier self-energy, the transverse, and the longitudinal polarization functions are given by

$$\Sigma_{ab}(\underline{1}\,\underline{2}) = -i\hbar e G_{ac}(\underline{1}\,\underline{3})W(\underline{4}\,\underline{1})\gamma_{cb}(\underline{3}\,\underline{2}\,\underline{4})$$
$$-i\hbar\vec{\Pi}(\underline{1}\,\underline{1}')G_{ac}(\underline{1}\,\underline{3})\vec{D}(\underline{4}\,\underline{1}')\vec{\Gamma}_{cb}(\underline{3}\,\underline{2}\,\underline{4})|_{1=1'}, \tag{12a}$$

$$p(\underline{1}\ \underline{2})=\frac{\delta\rho_{\rm ind}(\underline{1})}{\delta\Phi_{\rm eff}(\underline{2})}, \tag{12b}$$

$$\vec{\vec{P}}(\underline{1}\ \underline{2})=-\frac{4\pi}{c}\frac{\delta\vec{J}_{\rm ind}(\underline{1})}{\delta\vec{A}_{\rm eff}(\underline{2})}, \tag{12c}$$

where we have introduced the longitudinal $\gamma$ and transverse $\Gamma$ vertex functions,

$$\gamma_{ba}(\underline{1}\ \underline{2}\ \underline{3})=\frac{\delta G^{-1}_{ba}(\underline{1}\ \underline{2})}{\delta\Phi_{\rm eff}(\underline{3})},$$

$$\vec{\Gamma}_{ba}(\underline{1}\ \underline{2}\ \underline{3})=-\frac{4\pi}{c}\frac{\delta G^{-1}_{ba}(\underline{1}\ \underline{2})}{\delta\vec{A}_{\rm eff}(\underline{3})}, \tag{13}$$

which are obtained upon substitution into the Dyson equations,

$$\gamma_{ba}(\underline{1}\ \underline{2}\ \underline{3})=-e\delta_{ba}\delta(\underline{1}\ \underline{3})\delta(\underline{1}\ \underline{2})+\frac{\delta\Sigma_{ba}(\underline{1}\ \underline{2})}{\delta G_{cd}(\underline{4}\ \underline{5})}G_{cg}(\underline{4}\ \underline{6})\times\gamma_{gf}(\underline{6}\ \underline{7}\ \underline{3})G_{fd}(\underline{7}\ \underline{5}), \tag{14a}$$

$$\vec{\Gamma}_{ba}(\underline{1}\ \underline{2}\ \underline{3})=-\frac{4\pi e}{c^2}\vec{\Pi}(\underline{1}\ \underline{1}')\delta_{ba}\delta(\underline{1}\ \underline{3})\delta(\underline{1}\ \underline{2})|_{1=1'}+\frac{\delta\Sigma_{ba}(\underline{1}\ \underline{2})}{\delta G_{cd}(\underline{4}\ \underline{5})}G_{cg}(\underline{4}\ \underline{6})\vec{\Gamma}_{gf}(\underline{6}\ \underline{7}\ \underline{3})G_{fd}(\underline{7}\ \underline{5}). \tag{14b}$$

The induced particle and current densities are expressed in terms of the carrier Green's functions by

$$\rho_{{\rm ind},a}(\underline{1})=-i\hbar eG_{aa}(\underline{1}\ \underline{1}^{\pm}), \tag{15a}$$

$$\vec{J}_{{\rm ind},ab}(\underline{1})=-ie\hbar\vec{\Pi}(\underline{1}\ \underline{1}^{\pm})G_{ab}(\underline{1}\ \underline{1}^{\pm}). \tag{15b}$$

Detailed band-structure and quantum-confinement effects are included in the theory through the term $h_{\rm eff}$ in the free-carrier propagator $G_0^{-1}$, and also in the optical transition selection rules described by the matrix elements of the velocity operator, $\vec{\Pi}(\underline{1}\ \underline{2})=[\vec{\Pi}(\underline{1})+\vec{\Pi}^*(\underline{2})]/2=\hbar[\nabla(1)-\nabla(2)]/2im_0$. The carrier self-energy $\Sigma$ leads to band-gap renormalization, includes dynamic effects such as corrections beyond Hartree-Fock scattering rates in the carrier's kinetics, and enables the description of bound states (excitons) in the spectral density of carriers, defining the degree of ionization. The longitudinal polarization function $p$ is responsible for (plasmon) screening of the Coulomb interaction. Furthermore, it describes dynamical screening, screening by excitons, plasmon kinetics and the buildup of screening, although these topics will not be addressed in this paper. The transverse polarization function $\vec{\vec{P}}$ yields the excitation-dependent absorption coefficient and refractive index, and defines scattering rates (generation and/or recombination, and absorption and/or emission) in the photon kinetics. It is responsible for the inclusion of bound states (excitons) in the photons spectral density.

### B. Bethe-Salpeter equation

The Bethe-Salpeter equation for the transverse polarization function presented below allows the inclusion of excitonic corrections in the spectral density of photons. We give a general derivation, valid for both nonequilibrium and equilibrium conditions, and present solutions for the steady-state limit that are numerically solved and compared with experiments in Sec. IV. We start by rewriting the two-point tensor in Eq. (12c) in terms of a three-point vector,

$$\vec{\vec{P}}(\underline{1}\ \underline{2})=\frac{4\pi e^2}{c^2}\vec{\Pi}(\underline{1}\ \underline{1}^{\pm})\vec{\mathcal{L}}_{ab}(\underline{1}\ \underline{1}^{\pm}\ \underline{2}), \tag{16a}$$

$$\vec{\mathcal{L}}_{ab}(\underline{1}\ \underline{1}'\ \underline{2})=\frac{i\hbar c}{e}\frac{\delta G_{ab}(\underline{1}\ \underline{1}')}{\delta\vec{A}_{\rm eff}(\underline{2})}. \tag{16b}$$

Making use of the chain rule for functional derivatives, we obtain

$$\vec{\mathcal{L}}_{ab}(\underline{1}\ \underline{1}'\ \underline{2})=-G_{ac}(\underline{1}\ \underline{3})\frac{\delta G^{-1}_{cd}(\underline{3}\ \underline{4})}{\delta\vec{A}_{\rm eff}(\underline{2})}G_{db}(\underline{4}\ \underline{1}'). \tag{17}$$

Combining Eqs. (8a), (10a), (11), and further application of the chain rule, yields

$$\vec{\mathcal{L}}_{ab}(\underline{1}\ \underline{1}'\ \underline{2})=\vec{\mathcal{L}}_{0,ab}(\underline{1}\ \underline{1}'\ \underline{2})+G_{ac}(\underline{1}\ \underline{3})G_{db}(\underline{4}\ \underline{1}')\frac{\delta\Sigma_{cd}(\underline{3}\ \underline{4})}{\delta G_{fg}(\underline{5}\ \underline{6})}\vec{\mathcal{L}}_{fg}(\underline{5}\ \underline{6}\ \underline{2}), \tag{18}$$

where we have introduced the random phase approximation (RPA) transverse polarization vector function,

$$\vec{\mathcal{L}}_{0,ab}(\underline{1}\ \underline{1}'\ \underline{2})=-i\hbar\vec{\Pi}(\underline{2})G_{ac}(\underline{1}\ \underline{2})G_{db}(\underline{2}\ \underline{1}'). \tag{19}$$

Note that we sum over $c,d$ in Eq. (19), and use the same sum convention in the other RPA quantities defined below. Equation (18) can be more easily analyzed if expressed in terms of scalar quantities. That is possible by rewriting the transverse polarization vector function as

$$\vec{\mathcal{L}}_{ab}(\underline{1}\ \underline{1}'\ \underline{2})=\vec{\Pi}(\underline{2})\mathcal{P}_{ab}(\underline{1}\ \underline{1}'\ \underline{2}), \tag{20}$$

which satisfies the (scalar) Bethe-Salpeter equation,

$$\mathcal{P}_{ab}(\underline{1}\ \underline{1}'\ \underline{2})=\mathcal{P}_{0,ab}(\underline{1}\ \underline{1}'\ \underline{2})+-i\hbar G_{ac}(\underline{1}\ \underline{3})G_{db}(\underline{4}\ \underline{1}')\times\frac{\delta\Sigma_{cd}(\underline{3}\ \underline{4})}{\delta G_{fg}(\underline{5}\ \underline{6})}\mathcal{P}_{fg}(\underline{5}\ \underline{6}\ \underline{2}), \tag{21}$$

and $\mathcal{P}_{0,ab}(\underline{1}\ \underline{1}'\ \underline{2})=-i\hbar G_{ac}(\underline{1}\ \underline{2})G_{db}(\underline{2}\ \underline{1}')$. The equation above is exact, expressed in terms of a generalized potential

$i\hbar\, K_{cdfg}(\underline{3}\,\underline{4}\,\underline{5}\,\underline{6}) = \delta\Sigma_{cd}(\underline{3}\,\underline{4})/\delta G_{fg}(\underline{5}\,\underline{6})$. Systematic approximations can be obtained by successive iteration on the self-energy. For computational purposes, it will be helpful to use a four-point function. We start by expressing Eq. (21) under operator notation,

$$\mathcal{P}_{ab}(\underline{1}\,\underline{1}'\,\underline{2}) = \mathcal{O}^{-1}_{abfg}(\underline{1}\,\underline{1}'\,\underline{5}\,\underline{5}')\mathcal{P}_{0,fg}(\underline{5}\,\underline{5}'\,\underline{2}). \quad (22)$$

The operator $\mathcal{O}$ and it's inverse $\mathcal{O}^{-1}$ are given by

$$\mathcal{O}_{abfg}(\underline{1}\,\underline{1}'\,\underline{5}\,\underline{5}') = \delta(\underline{1}\,\underline{5})\delta(\underline{1}'\,\underline{5}')\delta_{af}\delta_{bg} + i\hbar G_{ac}(\underline{1}\,\underline{3})G_{db}(\underline{4}\,\underline{1}') \times K_{cdfg}(\underline{1}\,\underline{1}'\,\underline{5}\,\underline{5}'), \quad (23a)$$

$$\mathcal{O}^{-1}_{abcd}(\underline{1}\,\underline{1}'\,\underline{5}\,\underline{5}')\mathcal{O}^{1}_{cdfg}(\underline{5}\,\underline{5}'\,\underline{2}\,\underline{2}') = \mathcal{O}^{1}_{abcd}(\underline{1}\,\underline{1}'\,\underline{5}\,\underline{5}')\mathcal{O}^{-1}_{cdfg}(\underline{5}\,\underline{5}'\,\underline{2}\,\underline{2}') = \delta(\underline{1}\,\underline{2})\delta(\underline{1}'\,\underline{2}')\delta_{af}\delta_{bg}. \quad (23b)$$

At this point, we define the four-point quantities,

$$\mathcal{P}_{0,ab}(\underline{1}\,\underline{1}'\,\underline{2}\,\underline{2}') = -i\hbar G_{ac}(\underline{1}\,\underline{2})G_{db}(\underline{2}'\,\underline{1}'), \quad (24a)$$

$$\mathcal{P}_{ab}(\underline{1}\,\underline{1}'\,\underline{2}\,\underline{2}') = \mathcal{O}^{-1}_{abfg}(\underline{1}\,\underline{1}'\,\underline{5}\,\underline{5}')\mathcal{P}_{0,fg}(\underline{5}\,\underline{5}'\,\underline{2},\underline{2}'). \quad (24b)$$

Direct application of the operator $\mathcal{O}$ on Eq. (24b) gives rise to the Bethe-Salpeter equation for the four-point polarization,

$$\mathcal{P}_{ab}(\underline{1}\,\underline{1}'\,\underline{2}\,\underline{2}') = \mathcal{P}_{0,ab}(\underline{1}\,\underline{1}'\,\underline{2}\,\underline{2}') - G_{ac}(\underline{1}\,\underline{3})G_{db}(\underline{4}\,\underline{1}') \times K_{cdfg}(\underline{3}\,\underline{4}\,\underline{5}\,\underline{6})\mathcal{P}_{fg}(\underline{5}\,\underline{6}\,\underline{2}\,\underline{2}'). \quad (25)$$

Note that, by construction, $\mathcal{P}_{ab}(\underline{1}\,\underline{2}) = \mathcal{P}_{ab}(\underline{1}\,\underline{1}\,\underline{2}) = \mathcal{P}_{ab}(\underline{1}\,\underline{1}\,\underline{2}\,\underline{2})$. If the RPA is used for $\Sigma$, by taking only the first term on the right-hand side of Eqs. (14a) and (14b), the effective potential reads

$$K_{cdfg}(\underline{3}\,\underline{4}\,\underline{5}\,\underline{6}) = i\hbar\left[e^2 W(\underline{4}\,\underline{3}) - \frac{e^2}{c}\vec{\Pi}(\underline{3}\,\underline{3}')\cdot\vec{D}(\underline{3}\,\underline{5})\cdot\vec{\Pi}(\underline{4})\right] \times \delta_{cf}\delta_{dg}\delta(\underline{3}-\underline{5})\delta(\underline{4}-\underline{6}). \quad (26)$$

In what follows, we keep only the longitudinal contribution, $K_{cdfg}(\underline{3}\,\underline{4}\,\underline{5}\,\underline{6}) \approx i\hbar e^2 W(\underline{4}\,\underline{3})\ \ \delta_{cf}\delta_{dg}\ \ \delta(\underline{3}-\underline{5})\delta(\underline{4}-\underline{6})$, which gives rise to the more tractable equation,

$$\mathcal{P}_{ab}(\underline{1}\,\underline{1}'\,\underline{2}\,\underline{2}') = \mathcal{P}_{0,ab}(\underline{1}\,\underline{1}'\,\underline{2}\,\underline{2}') + i\hbar e^2 G_{ac}(\underline{1}\,\underline{3}) \times G_{db}(\underline{4}\,\underline{1}')W(\underline{3}\,\underline{4})\mathcal{P}_{cd}(\underline{3}\,\underline{4}\,\underline{2}\,\underline{2}'). \quad (27)$$

At this point, we specify the equations for the incoherent electric field case. The interband components of the carrier Green's function are then left out, since they are driven by the average field, which in this case is zero.[7,10] Furthermore, nondiagonal intraband terms are also not considered, consistently with the approximations used in the computation of Coulomb matrix elements (see the Appendix).[11] In summary, $G_{ab}(\underline{1}\,\underline{1}') \approx \delta_{ab}G_{aa}(\underline{1}\,\underline{1}')$. We further switch form the conduction-valence band to the electron-hole picture, the notation of which is also discussed in the Appendix. Further defining $W_{eh}(\underline{1}\,\underline{2}) = -\hbar e^2 W(\underline{1}\,\underline{2})$, Eq. (27) simplifies to (no sum over band indices)

$$\mathcal{P}_{eh}(\underline{1}\,\underline{1}'\,\underline{2}\,\underline{2}') = \mathcal{P}_{0,eh}(\underline{1}\,\underline{1}'\,\underline{2}\,\underline{2}') + iG_{ee}(\underline{1}\,\underline{3})G_{hh}(\underline{1}'\,\underline{4}) \times W_{eh}(\underline{3}\,\underline{4})\mathcal{P}_{eh}(\underline{3}\,\underline{4}\,\underline{2}\,\underline{2}'), \quad (28a)$$

$$\mathcal{P}_{eh}(\underline{1}\,\underline{1}'\,\underline{2}\,\underline{2}') = \mathcal{P}_{0,eh}(\underline{1}\,\underline{1}'\,\underline{2}\,\underline{2}') - \hbar G_{ee}(\underline{1}\,\underline{3})G_{hh}(\underline{1}'\,\underline{4}) \times T_{eh}(\underline{3}\,\underline{4}\,\underline{5}\,\underline{6})G_{ee}(\underline{5}\,\underline{2})G_{hh}(\underline{6}\,\underline{2}'), \quad (28b)$$

where we have introduced the electron-hole quantity,

$$\mathcal{P}_{0,eh}(\underline{1}\,\underline{1}'\,\underline{2}\,\underline{2}') = -i\hbar G_{ee}(\underline{1}\,\underline{2})G_{hh}(\underline{1}'\,\underline{2}'), \quad (29)$$

and have defined (under the integration sign) the $T$ matrix

$$W_{eh}(\underline{3}\,\underline{4})\mathcal{P}_{eh}(\underline{3}\,\underline{4}\,\underline{2}\,\underline{2}') = i\hbar T_{eh}(\underline{3}\,\underline{4}\,\underline{5}\,\underline{6}) \times G_{ee}(\underline{5}\,\underline{2})G_{hh}(\underline{6}\,\underline{2}'). \quad (30)$$

Substitution of Eq. (30) into Eq. (27) yields the $T$-matrix equation,

$$T_{eh}(\underline{1}\,\underline{2}\,\underline{1}'\,\underline{2}') = W_{eh}(\underline{1}\,\underline{2})\delta(\underline{1}\,\underline{1}')\delta(\underline{2}\,\underline{2}') + iW_{eh}(\underline{1}\,\underline{2})G_{ee}(\underline{1}\,\underline{3}) \times G_{hh}(\underline{1}'\,\underline{4})T_{ab}(\underline{3}\,\underline{4}\,\underline{1}'\,\underline{2}'). \quad (31)$$

The screened ladder approximation allows us to write the carrier self-energy as the sum of an RPA term and a correlation contribution, which can also be expressed by means of the $T$ matrix defined by Eq. (31) (see the Appendix),

$$\Sigma_{ee}(\underline{1}\,\underline{1}') = \Sigma^{\mathrm{HF}}_{ee}(\underline{1}\,\underline{1}') + \Sigma^{c}_{ee}(\underline{1}\,\underline{1}'). \quad (32)$$

The notation $1 = \vec{r}_1, t_1$ means that time runs under a (Keldysh) contour from $-\infty$ to $+\infty$ on a positive branch, $t_1 = t_+$ and back on a negative contour from $+\infty$ to $-\infty$, and thus $t_1 = t_-$.[9] The nonequilibrium approach can describe time-dependent phenomena on an ultrafast scale. In this paper, however, we concentrate on steady-state results, which means that all quantities depend only on the relative time $\tau = t_1 - t_2$. The optical spectra and recombination rates in the frequency domain are thus obtained after a Fourier transform with respect to the relative time, taken in the physical limit $\tau_+ = \tau_-$. The photons are in a nonequilibrium state while the carriers are in quasiequilibrium among the various subbands.

The polarization function has been computed self-consistently, first only with the RPA bubble, then with $T$-matrix corrections and RPA self-energy, and finally with the full self-energy, for bulk 3D,[13] and MQW's in the limit of decoupled superlattices. The full details of the numerical procedure will be given elsewhere.[12] At room temperatures, and down to 77 K, the inclusion of $T$-matrix corrections in the self-energy does not change the spectra. In other words,

the excitonic effects are well described by the Bethe-Salpeter equation with RPA propagators, and all numerical results presented here are on that level of approximation. We expect deviations only at very low temperatures, and progress in this direction is under way.

Equations (8b) and (9a) make it clear that the required quantity in our computations is actually $\mathcal{P}_{eh}(\underline{1}\,\underline{2})$, which we will treat in the limit of a two-point in time, four-point in space function, namely, $\mathcal{P}_{eh}(R_1R_{1'}R_2R_{2'},t_{\underline{1}},t_{\underline{2}})|_{R_{1'}=R_1,R_{2'}=R_2}$.

The Bethe-Salpeter or $T$-matrix equation reduces to the Wannier exciton equation in the limiting case of vanishing carrier populations. For a bulk system with parabolic bands, in either $2d$ or $3d$, the excitonic spectrum is recovered. However, with a finite carrier density, the Coulomb potential is screened, the band gap is modified, and carrier-carrier scattering takes place. The Bethe-Salpeter or $T$-matrix equations no longer correspond to a simple excitonic picture and now describe a many-particle system that in this sense goes beyond the exciton picture.

### III. COUPLED BAND QUANTUM WELLS

The expressions presented above are general, do not depend on the dimensionality of the system, and can be applied to bulk, isolated multiple quantum wells, coherently coupled superlattices, quantum wires, and dots. In order to refer to specific experimental data found in the literature, we apply them to the quantum-well case at steady state. The quantum confinement and valence-band coupling require the diagonalization of the corresponding Luttinger Hamiltonian. We consider only constituent materials in which the band gap is sufficiently large to decouple the conduction bands, which are then parabolic. Each conduction subband is then described by the $m_J=\pm 1/2$ projection of the electron spin $\sigma$, and a quantization index $j=c_1c_2\ldots$, as well as the in-plane quasimomentum $\vec{k}$. We keep the notation as simple as possible and condense the quantum numbers in a single label, $n=\{\sigma j\}$. The coupled valence bands each have a heavy $m_J=\pm 3/2$ and a light-hole component $m_J=\pm 1/2$. In other words, in this case $n=\{pj\}$, $j=v_1v_2\ldots$. The band labels $a,b,c\ldots$ of the preceding sections will from now on be replaced by the more specific $n_1,n_2,n_3\ldots$. The block diagonalization label $p$ reduces to a spin label $\sigma$ in the absence of band coupling.[11] The eigenstates of the free-carrier Hamiltonian, $H_0$, can be written as

$$\phi_{n\vec{k}}=\phi_{\sigma j\vec{k}}(\vec{R})=\frac{1}{S^{1/2}}e^{i\vec{k}\cdot\vec{r}}g_j(z)\ w_{\sigma j}, \tag{33a}$$

$$\phi_{n\vec{k}}=\phi_{pj\vec{k}}(\vec{R})=\frac{1}{S^{1/2}}e^{i\vec{k}\cdot\vec{r}}[\xi_{Hpj\vec{k}}(z)w_{Hp}+\xi_{Lpj\vec{k}}(z)w_{Lp}]. \tag{33b}$$

Here, $S$ is the sample area, and the in-plane and growth direction components of the position vector $\vec{R}$ are given by $(\vec{r},z)$. The subscripts $H$ and $L$ denote, respectively, the heavy- and light-hole components of the coupled band state. $w_{Hp}$, $w_{Lp}$, and $w_{\sigma j}$ are fast-varying lattice-periodic functions. The envelope functions $\xi_{Lpj\vec{k}}(z)$, $\xi_{Hpj\vec{k}}(z)$, and $g_j(z)$ are obtained from the diagonalization of $H_0$. The unrenormalized dispersion relations for conduction and nonparabolic valence bands are given, respectively, by $\hbar\epsilon^e_{kj}=\hbar\epsilon^e_j+\hbar^2k^2/2m^*_e$ and $\hbar\epsilon^v_{kj}$. Note that, away from $k=0$, the top valence band has a light-hole component, which can give rise to structures in the TM absorption and/or gain and emission spectra, in the spectral vicinity of the transition usually assigned as the ''electron–heavy hole,'' which would not be present if band-coupling effects were not taken into consideration. In that simplified case, features in the TM spectra appear only at the pure electron–light-hole transitions.

Following the prescription presented in Ref. 7 for a homogeneous approximation for the excited medium, we use the QW Hamiltonian basis of eigenstates to expand Fourier-transformed Keldysh components (see the Appendix), without the by now unnecessary tensor and vector notation,

$$P^\lambda(\omega)=\sum_{\vec{k},n_1,n_2}\Pi_{n_1,n_2}(k)\mathcal{L}^\lambda_{n_1,n_2}(k,\omega),$$

$$\mathcal{L}^\lambda_{n_1,n_2}(k,\omega)=\sum_{\vec{k}',n_3,n_4}\Pi_{n_3,n_4}(k')\mathcal{P}^\lambda\begin{pmatrix}n_1n_2n_3n_4\\ kkk'k'\end{pmatrix}(\omega), \tag{34}$$

where $\lambda=<r,a$ denotes, respectively, the backward, retarded, and advanced Keldysh components, $n_i$ includes all quantum numbers describing the solutions of the parabolic conduction and coupled valence bands, and

$$\mathcal{P}^\lambda\begin{pmatrix}n_1n_2n_3n_4\\ kkk'k'\end{pmatrix}(\omega)=\int d\vec{R}_3d\vec{R}_4\phi^*_{n_1\vec{k}}(\vec{R}_3)\phi_{n_2\vec{k}}(\vec{R}'_3)\mathcal{P}^\lambda(\vec{R}_3\vec{R}'_3\vec{R}_4\vec{R}'_4)(\omega)\phi_{n_3\vec{k}'}(\vec{R}_3)\phi^*_{n_4\vec{k}'}(\vec{R}_4)|_{\substack{\vec{R}_3=\vec{R}'_3\\ \vec{R}_4=\vec{R}'_4}}. \tag{35}$$

The backward ($\lambda=<$) Keldysh component is related to the carrier recombination rates and thus to the luminescence spectrum, while the retarded ($\lambda=r$) component contains spectral information. We can show (see the Appendix) that $\mathcal{L}^r$ satisfies an equation with the same structure of the semiconductor Bloch equation for the interband polarization,[4,14]

$$\mathcal{L}^r_{n_1,n_2}(k,\omega)=\mathcal{L}^r_{0,n_1,n_2}(k,\omega)-\frac{1}{\Pi_{n_1,n_2}(k)}\sum_{\vec{k}'}\mathcal{L}^r_{0,n_1,n_2}(k,\omega)W\begin{pmatrix}n_1n_2n_1n_2\\ \vec{k}-\vec{k}'\end{pmatrix}\mathcal{L}^r_{n_1,n_2}(k',\omega). \tag{36}$$

The driving term $\mathcal{L}^r_{0,n_1,n_2}(k,\omega)$ has real and imaginary parts. The imaginary part is directly computed from the relation $2i\ \mathrm{Im}\{\mathcal{L}^r_{0,n_1,n_2}(k,\omega)\}=\mathcal{L}^>_{0,n_1,n_2}(k,\omega)-\mathcal{L}^<_{0,n_1,n_2}(k,\omega)$, where

$$\mathcal{L}^{\lessgtr}_{0,n_1n_2}(k,\omega)=i\hbar\Pi_{n_1n_2}\int\frac{d\omega'}{2\pi}G^{\lessgtr}_{n_1n_1}(k,\omega')G^{\lessgtr}_{n_2n_2}(k,\omega-\omega')$$

$$=i\hbar\Pi_{n_1n_2}\int\frac{d\omega'}{2\pi}\hat{G}_{n_1n_1}(k,\omega')\hat{G}_{n_2n_2}(k,\omega-\omega')\begin{pmatrix}f_e(\omega')f_h(\omega-\omega')\\[1-f_e(\omega')][1-f_h(\omega-\omega')]\end{pmatrix}. \quad (37)$$

The spectral function $\hat{G}$ is given by

$$\hat{G}_{nn}(k,\omega)=\frac{2\hbar\Gamma_n}{(\hbar\omega-\hbar e_n)^2+\hbar^2\Gamma_n^2}, \quad (38)$$

where

$$\hbar e_n=\hbar\epsilon_n-\mathrm{Re}\{\Sigma^r_{nn}(k,\omega)\}$$

and

$$\hbar\Gamma_n=-\mathrm{Im}\{\Sigma^r_{nn}(k,\omega)\}$$

denote, respectively, the renormalized energies and the dephasing rate. We have considered the resonant case in which $n_1$ and $n_2$ denote, respectively, electron and hole subbands. For $\delta$-function-like spectral functions, we then have $\omega\approx e_{n_1}+e_{n_2}$. A Kramers-Kronig transformation yields $\mathrm{Re}\{\mathcal{L}^r_{0,n_1,n_2}(k,\omega)\}$. Here, $f_a(\omega)=1/(\exp\beta[\hbar\omega-\mu_a]+1)$ is the Fermi distribution for a quasiparticle of type $a$, characterized by the quasichemical potential $\mu_a$, which is determined self-consistently (see the Appendix for a discussion). Combining Eqs. (34)–(38), and using the KMS relation,[1,6] as discussed in the Appendix, we obtain $P^{\gtrless}$ once $\mathrm{Im}\{P^r\}$, has been computed,

$$P^<(\omega)=\frac{-2i\ \mathrm{Im}\{P^r(\omega)\}}{1-\exp(\beta(\hbar\omega-\mu))}, \quad (39)$$

where $\mu=\mu_e+\mu_h$ is the total chemical potential. The resulting expressions can then be combined with the solutions of the photon Green's-function propagator $D^<$, which are directly related to the quantum-mechanical Poynting vector, and thus lead to light-emission spectra.[10,7] Note that in both TE $D^<_{ij}(k,\omega)=D^<(k,\omega)\delta_{i,y}\delta_{j,y}$ (propagation along $\hat{x}$) and TM $D^<_{ij}(k,\omega)=D^<(k,\omega)\delta_{i,z}\delta_{j,z}$ (propagation along $\hat{y}$) modes, the three-dimensional optical cavity can be reduced to an effective one-dimensional resonator, with the output spectrum given by

$$I(\omega)=\frac{\hbar\omega^2}{4\pi^2c}\tan^2\theta iP^<(\omega)L\mathcal{F}_L(\omega), \quad (40)$$

where the resonator mode structure is given by

$$\mathcal{F}_L(\omega)=\frac{1}{|1-r^2|^2}\frac{1}{|n(\omega)|^2}\frac{1}{|n(\omega)+1|^2}e^{-(\omega/c)n_2(\omega)L}\mathcal{J}_L(q). \quad (41)$$

Here, $\mathcal{J}_L(q)$ is a slowly varying function of the cavity length, and $n_2(\omega)$ is the imaginary part of the complex refractive index $n(\omega)$. It is computed by means of the relation $n_2\sim-c^2/[2\omega^2\sqrt{\epsilon(\infty)}]\mathrm{Im}\ P^r$, and the background dielectric constant $\epsilon(\infty)$ can be found in material parameter tables.[10,7] If we assume the samples to be antireflection coated, resonator effects play no role and the emitted light field intensity per unit length can be simplified, $I(\omega)\sim\hbar\omega^2/4\pi^2ciP^<(\omega)$. The absorption reads $\alpha(\omega)\sim c/[2\omega\sqrt{\epsilon(\infty)}]\mathrm{Im}\ P^r(\omega)$.

## IV. NUMERICAL RESULTS AND DISCUSSION

Figure 1 shows absorption spectra, $\alpha(\omega)=c/[2\omega\sqrt{\epsilon(\infty)}]\mathrm{Im}\ P^r(\omega)$, of a 50 Å GaAs/$Al_xGa_{1-x}$As QW at 300 K and corresponding luminescence spectra. In contrast to Refs. 2 and 3, our theory provides spectra for different polarizations of the electromagnetic field including all relevant band-structure effects. Notably, to the best of our knowledge for the first time, we predict a structure at the spectral position corresponding to a heavy hole in the TM spectra. It appears in our low-density GaAs data in Fig. 1(b). The inset shows the effect more clearly. We have chosen a slightly strain-relieved, 60 Å $In_{0.2}Ga_{0.8}As$/GaAs quantum well. Strain relief may occur, due to sample imperfections, or when a relatively large number of wells in the multiple-quantum-well sample gives rise to a thick active layer. Further lattice accommodation occurs, and the in-plane component of the strain tensor is no longer well described by the simple expression $\epsilon=(d_b-d_w)/d_b$, where $d_w$ and $d_b$ denote, respectively, the well and barrier widths. It is beyond the scope of this paper to make a first-principles model for the strain relief. Instead, we follow Ref. 15, and introduce a strain-relaxation parameter $\gamma$, such that $\epsilon=(1-\gamma)(d_b-d_w)/d_b$, and use this value in the numerical algorithm that solves the Luttinger Hamiltonian. The confining potential is then deeper and it is possible to have light holes bound in the quantum well, thus leading to strong band coupling.[16] We have multiplied the TM spectrum by a factor 20 for a better comparison. The example corresponds to the data obtained in Ref. 17, where a predominantly TE spectral peak has been measured at 1.279 eV and a predominantly TM peak at 1.32–1.33 eV. It is due to the fact that the top valence band (heavy hole at $k=0$) acquires a light-hole component due to band coupling, which is further enhanced by the Coulomb interaction. It also manifests as a bump in the low-energy side of the TM absorption as seen in Fig. 1(a). Without the combined Coulomb and band-coupling effects, these structures would not be present. Also, in agreement with experimental data,[18] the photoluminescence output increases with increasing carrier density. The amplified spontaneous emission that evolves into lasing is consistently described by our approach. Another important feature of our calculations is the gain line shape. It has been recently demonstrated that the spurious absorption below the gain region, which appears if the Pauli-blocking factor is written under the quasiparticle approximation, i.e., with the Fermi functions evaluated at the

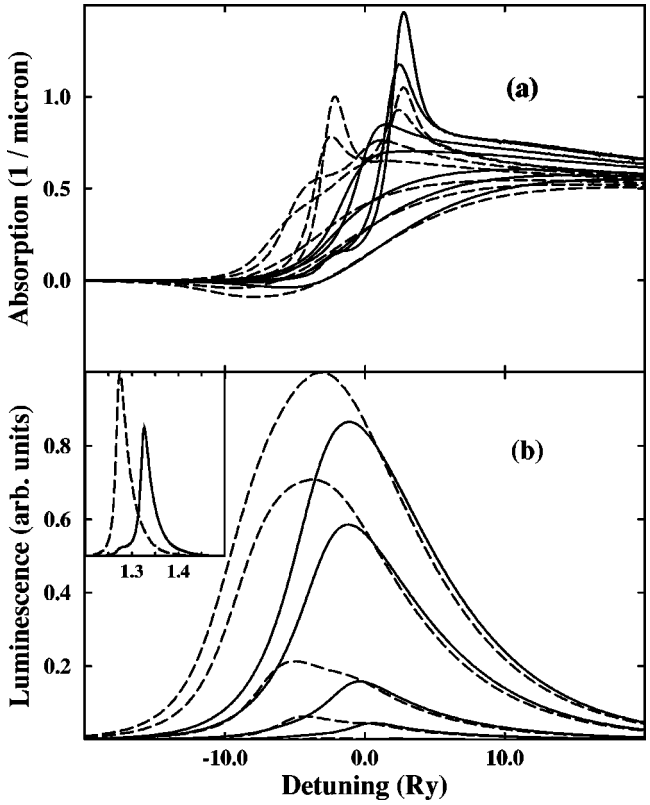


FIG. 1. (a) TE (dashed) and TM (solid) absorption, with corresponding photoluminescence (PL) spectra, (b) for a 50 Å GaAs-$Al_{0.23}Ga_{0.77}As$ QW as a function of detuning with respect to the free-carrier band gap at 300 K. From top to bottom the carrier densities for absorption and PL are $N=0,0.1,0.5,1.0,2.0,2.5,3.0$ and $2.5,2.0,1.0,0.5,0.1\times10^{18}$ carriers/cm$^3$. The inset compares the TE and TM luminescence spectra of a strain-relieved, 60 Å $In_{0.2}Ga_{0.8}As/GaAs$ quantum well at 300 K. The carrier density used is $N=5.0\times10^{17}$ carriers/cm$^3$. The $x$ axis is in eV (TM spectrum X20).

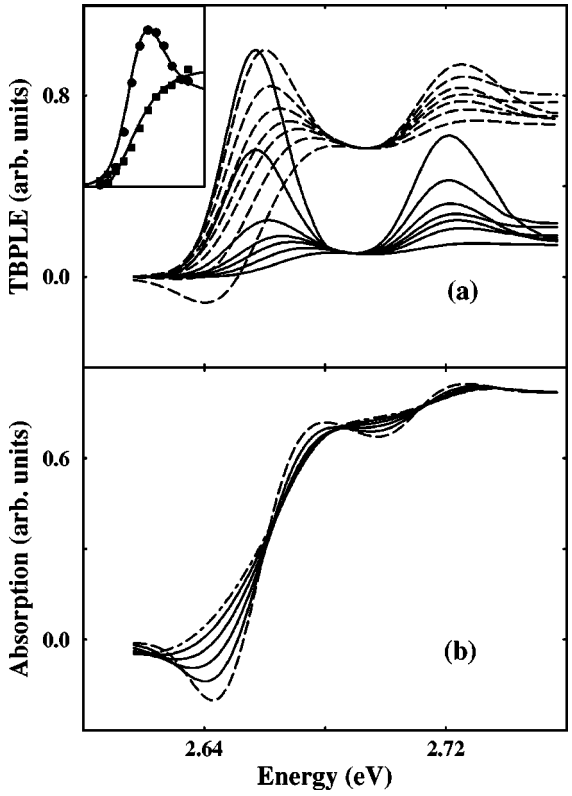


FIG. 2. (a) Two-beam photoluminescence excitation spectroscopy spectra (solid) for a 30 Å ZnCdSe/ZnSSe QW at at plasma temperature $T_{pl}=77$ K. From top to bottom the pump-generated carrier densities are $N=0.42,0.63,0.84,1.04,1.25,1.67,2.51\times10^{18}$ carriers/cm$^3$. Dashed: corresponding absorption spectra, with the same normalization. In (b), the high-density absorption and/or gain spectra are shown, and from the dashed to the dot-dashed curve, the inhomogeneous broadening due to alloy concentration fluctuation is increased. The inset shows a comparison of our theory (solid) with the TBPLE experiments (symbols) from Ref. 21 for a 100 Å sample.

dispersion relations, $f_e(e_e(k))$, $f_h(e_h(k))$, can be eliminated by considering nondiagonal dephasing terms in the (coherent) polarization.[19] Another consequence of the quasiparticle approximation, so far not discussed in the literature, is the development of negative luminescence on the high-energy side of the spectra. None of these artifacts appear in the alternative approach presented here, since by making sure that the polarization function satisfies the KMS condition, high $k$ value contributions that ultimately give rise to the artifacts are eliminated. Furthermore, since our theory automatically guarantees that the switch from absorption to gain occurs exactly at the chemical potential, the technique proposed in Ref. 20 to extract the gain spectra from spontaneous emission data can be used safely without a discrepancy between ''experimental'' and ''computed'' total chemical potential differences. Note that, for the comparison with that specific experiment, the full chemical potential, which describes the exciton gas at low carrier densities, should be used, and it can be self-consistently computed through Eq. (E2b). However, for the purposes of this paper, we can use the self-consistent solution of Eq. (E3) without ambiguities, since, as previously discussed, in the temperature range considerer here, the introduction of $T$-matrix corrections in the spectral density of carriers does not alter the optical spectra.

Figure 2 depicts two-beam photoluminescence excitation spectroscopy (TBPLE) and the corresponding absorption spectra, with the same normalization, in good qualitative agreement with experiments.[21] The numerical method follows directly the experimental technique. The linear absorption is computed and from that, assuming that all the light is converted into carriers, the pump-generated density at steady state can be calculated, using a lifetime $\tau=100$ ps. The pump energy is fixed at $\omega_{pu}$ and the luminescence, due to the pump only, is computed at the fixed energy $\omega_{det}$. Additional carriers are generated by the probe beam, which is absorbed according to the nonlinear absorption created by the pump. The luminescence due to both beams is detected at $\omega_{det}$, and the constant pump contribution is subtracted. The figures demonstrate that TBPLE and nonlinear absorption are qualitatively related, and the higher density curves illustrate the coexistence of gain and structures due to Coulomb correlations, which correspond to a ''bleached exciton,'' or better, to a strongly interacting electron-hole plasma. Note, however, that concentration and well-width fluctuations give rise to inhomogeneous broadening, usually larger for thinner quantum wells. Figure 2 also shows that, as the inhomogeneous broadening increases, the observed nonlinear spectra

loses the sharp ''excitonic features.'' In other words, under the presence of strong inhomogeneities, pump and probe experiments alone are not capable of identifying as ''excitonic'' or not the mechanism that yields gain, carrier, recombination, and thus lasing. In Ref. 22 we complement the brief discussion given here, by analyzing another sample, obtaining the same qualitative conclusion. We further present a systematic comparison between additional numerical results and experiments under wide temperature and excitation density conditions, further illustrating the relevance of the theoretical approach.

## V. SUMMARY

In summary, the first-principles theory for light emission and absorption in semiconductors presented here provides a technique to study Coulomb effects beyond RPA in semiconductors. It explains optical absorption, gain, and emission spectra consistently, and eliminates unphysical features by satisfying important sum rules. It further demonstrates the difficulty in analyzing optical experiments under the presence of strong inhomogeneities and demonstrates that TBPLE and nonlinear absorption are related, the first technique being advantageous if, e.g., a laser is to be studied under operation conditions, without the need to pierce a hole through the sample, and consequently destroy the device, as required for absorption measurements. We hope that this paper will stimulate detailed optical measurements in high-quality samples with pure homogeneous broadening in order to understand physical processes that are of general interest for solid-state physics by themselves and at the same time relevant for technological applications. The approach presented can also be used as the starting point for the realistic simulation of light-emitting and processing devices.

## ACKNOWLEDGMENTS

The authors thank T. Schmielau for a discussion comparing the self-energy used here with that presented in Ref. 13. This work has been supported by the Deutsche Forschungsgemeinschaft (DFG), ''Schwerpunktprogramm II-VI Halbleiter. Optoelektronik in blauen Spektralbereich.''

## APPENDIX A: THE BETHE-SALPETER EQUATION FOR THE RETARDED POLARIZATION

There is a linear dependence between the different Keldysh components of the Green's functions. Let $O$ represent the two-point Green's functions $(\vec{D},G,W)$ or their self-energies $(\vec{P},\Sigma,p)$. Then the retarded $(r)$, advanced $(a)$, forward $(>)$, and backward $(<)$ quantities are connected by the relations

$$O^r(12)=O^{++}(12)-O^{+-}(12)\equiv O^{++}(12)-O^{<}(12)$$
$$=O^{-+}(12)-O^{--}(12)\equiv O^{>}(12)-O^{--}(12), \tag{A1a}$$

$$O^a(12)=O^{++}(12)-O^{-+}(12)\equiv O^{++}(12)-O^{>}(12)$$
$$=O^{+-}(12)-O^{--}(12)\equiv O^{<}(12)-O^{--}(12). \tag{A1b}$$

The time integration follows the convention

$$\mathcal{T}(1^+\,3^+)=\int d(\underline{2})\mathcal{O}(1^+\,\underline{2})\mathcal{M}(\underline{2}\,3^+)$$
$$=\int d(2)[\mathcal{O}(1^+\,2^+)\mathcal{M}(2^+\,3^+)$$
$$-\mathcal{O}(1^+\,2^-)\mathcal{M}(2^-\,3^+)], \tag{A2a}$$

$$\mathcal{T}(1^+\,3^-)=\int d(\underline{2})\mathcal{O}(1^+\,\underline{2})\mathcal{M}(\underline{2}\,3^-)$$
$$=\int d(2)[\mathcal{O}(1^+\,2^+)\mathcal{M}(2^+\,3^-)$$
$$-\mathcal{O}(1^+\,2^-)\mathcal{M}(2^-\,3^-)], \tag{A2b}$$

$$\mathcal{T}(1^-\,3^-)=\int d(\underline{2})\mathcal{O}(1^-\,\underline{2})\mathcal{M}(\underline{2}\,3^-)$$
$$=\int d(2)[\mathcal{O}(1^-\,2^+)\mathcal{M}(2^+\,3^-)$$
$$-\mathcal{O}(1^-\,2^-)\mathcal{M}(2^-\,3^-)], \tag{A2c}$$

$$\mathcal{T}(1^-\,3^+)=\int d(\underline{2})\mathcal{O}(1^-\,\underline{2})\mathcal{M}(\underline{2}\,3^+)$$
$$=\int d(2)[\mathcal{O}(1^-\,2^+)\mathcal{M}(2^+\,3^+)$$
$$-\mathcal{O}(1^-\,2^-)\mathcal{M}(2^-\,3^+)]. \tag{A2d}$$

We eliminate the by now unnecessary subband indices for clarity. $\{a,b\}$ now denote branch indices along the Keldysh contour.[9] Starting from Eq. (27), and using static screening, which is diagonal in the branch indices, we can see that the different Keldysh components of the four-point in space, two-point in time transverse polarization function satisfy the equation

$$\mathcal{P}^{ab}(R_1R_1{}',R_2R_2{}',t_1t_2)=\mathcal{P}_0^{ab}(R_1R_1{}',R_2R_2{}',t_1t_2)$$
$$-\sum_\lambda\int dt_3dR_3R_4\mathcal{P}_0^{a\lambda}(R_1R_1{}',R_3R_3,t_1t_3)W(R_3R_4)\mathcal{P}^{\lambda b}(R_3\,R_4\,R_2\,R_2{}',t_3t_2), \tag{A3}$$

which we write, schematically, as

$$\mathcal{P}^{ab}=\mathcal{P}_0^{ab}-W\mathcal{P}_0^{a\lambda}\mathcal{P}^{\lambda b}, \tag{A4}$$

and consequently,

$$\begin{aligned}\mathcal{P}^r &= \mathcal{P}^{++} - \mathcal{P}^< \\ &= \mathcal{P}_0^{++} - \mathcal{P}_0^< - W\mathcal{P}_0^{++}\mathcal{P}^{++} + W\mathcal{P}_0^{++}\mathcal{P}^< + W\mathcal{P}_0^<\mathcal{P}^> - W\mathcal{P}_0^>\mathcal{P}^< \\ &= \mathcal{P}_0^r - W\mathcal{P}_0^{++}(\mathcal{P}^{++} - \mathcal{P}^<) + W\mathcal{P}_0^<(\mathcal{P}^> - \mathcal{P}^{--}) \\ &= \mathcal{P}_0^r - W\mathcal{P}_0^{++}\mathcal{P}^r + W\mathcal{P}_0^<\mathcal{P}^r \\ &= \mathcal{P}_0^r - W(\mathcal{P}_0^{++} - \mathcal{P}_0^<)\mathcal{P}^r = \mathcal{P}_0^r - W\mathcal{P}_0^r\mathcal{P}^r. \end{aligned} \tag{A5}$$

At steady state, we thus obtain

$$\mathcal{P}^{ab}(R_1R_{1'}R_2R_{2'},\omega) = \mathcal{P}_0^{ab}(R_1R_{1'}R_2R_{2'},\omega) - \int dR_3R_4\mathcal{P}_0^{a\lambda}(R_1R_{1'}R_3R_3,\omega)W(R_3R_4)\mathcal{P}^{\lambda b}(R_3R_4R_2R_{2'},\omega). \tag{A6}$$

At this point, we select a given linear polarization, and, as discussed in the main text, the tensor and vector notation can be dropped, and we may express the Keldysh components of the transverse polarization in the homogeneous approximation by[7]

$$P^{ab}(R_1R_2,\omega) = \frac{\delta(R_1 - R_2)}{\Omega}P^{ab}(\omega),$$

$$\begin{aligned}P^{ab}(\omega) &= \frac{4\pi ie\hbar}{c\Omega}\int dR_1dR_2\vec{\Pi}(R_1R_{1'})\mathcal{L}^{ab}(R_1R_{1'}R_2,\omega)|_{R_1=R_{1'}} \\ &= \frac{4\pi ie\hbar}{c\Omega}\int dR_1dR_2\Pi(R_1R_{1'})\Pi(R_2)\mathcal{P}^{ab}(R_1R_{1'}R_2R_2,\omega)|_{R_1=R_{1'}}. \end{aligned} \tag{A7}$$

If we now expand the polarization function in eigenstates of the free carrier Hamiltonian, defined in Eqs. (33a) and (33b), we obtain (the vector notation for position and momenta will not be used unless necessary)

$$\begin{aligned}P^{ab}(\omega) &= \frac{4\pi e^2\hbar}{c^2\Omega}\sum_{\substack{n_1n_2n_3n_4\\k_1k_2k_3k_4}}\mathcal{P}^{ab}\begin{pmatrix}n_1n_2n_3n_4\\k_1k_2k_3k_4\end{pmatrix} \\ &\quad\times(\omega)\int dR_1dR_2[\Pi(R_1R_{1'})\Pi(R_2)\phi_{n_1}(k_1R_1)\phi_{n_2}^*(k_2R_{1'})\phi_{n_3}(k_3R_2)\phi_{n_4}^*(k_4R_2)]|_{R_1=R_{1'}} \\ &= \frac{4\pi e^2\hbar}{c^2\Omega}\sum_{\substack{n_1n_2n_3n_4\\kk'}}\Pi_{n_1n_2}(k)\Pi_{n_3n_4}^*(k)\mathcal{P}^{ab}\begin{pmatrix}n_1n_2n_3n_4\\kkk'k'\end{pmatrix}(\omega). \end{aligned} \tag{A8}$$

The notation used for the matrix elements of a given operator, $\mathcal{O}$, means

$$\mathcal{O}\begin{pmatrix}n_1n_2n_3n_4\\k_1k_2k_3k_4\end{pmatrix} = \int d\vec{R}_3d\vec{R}_4\phi_{n_1\vec{k}_1}^*(\vec{R}_3)\phi_{n_2\vec{k}_2}(\vec{R}_3')\mathcal{O}(\vec{R}_3\vec{R}_3'\vec{R}_4\vec{R}_4')\phi_{n_3\vec{k}_3}(\vec{R}_3)\phi_{n_4\vec{k}_4}^*(\vec{R}_4)|_{\substack{\vec{R}_3=\vec{R}_3'\\\vec{R}_4=\vec{R}_4'}}. \tag{A9}$$

Equation (A6) for the retarded component thus reduces to

$$\mathcal{P}^r\begin{pmatrix}n_1n_2n_3n_4\\kkk'k'\end{pmatrix}(\omega) = \mathcal{P}_0^r\begin{pmatrix}n_1n_2n_3n_4\\kkk'k'\end{pmatrix}(\omega) - \sum_{\substack{m_1m_2m_3m_4\\q_1q_3q_4}}\mathcal{P}_0^r\begin{pmatrix}n_1n_2m_1m_2\\kkq_1q_1\end{pmatrix}(\omega)\mathcal{P}^r\begin{pmatrix}m_3m_4n_3n_4\\q_3q_4k'k'\end{pmatrix}(\omega)W\begin{pmatrix}m_1m_2m_3m_4\\q_1q_1q_1-q_3\end{pmatrix}, \tag{A10}$$

where we have used the relation (see Appendix B)

$$W\begin{pmatrix}m_1m_2m_3m_4\\q_1q_1q_3q_4\end{pmatrix} = \delta_{q_1-q_3}\delta_{q_1-q_4}W\begin{pmatrix}m_1m_2m_3m_4\\q_1q_1q_1-q_3\end{pmatrix}. \tag{A11}$$

As in Ref. 7, we keep only diagonal terms in the one-particle Green's functions, i.e., $G_{n_1n_2}(k,\omega)\sim\delta_{n_1,n_2}G_{n_1n_1}(k,\omega)$. Furthermore, we consider only the combination of indices that maximizes the screened potential matrix elements, namely

$$W\begin{pmatrix} m_1 m_2 m_3 m_4 \\ q_1 q_1 q_3 - q_4 \end{pmatrix} \sim \delta_{m_1,m_2}\delta_{m_1,m_2}\delta_{q_1,q_4} W\begin{pmatrix} m_1 m_2 m_1 m_2 \\ q_1 - q_3 \end{pmatrix}, \tag{A12}$$

and make an analogous approximation for $\mathcal{P}^r$ and $\mathcal{P}^{\gtrless}$, which leads to the equation (we can now use a simpler notation)

$$\mathcal{P}^r_{n_1,n_2}(k,\omega) = \mathcal{P}^r_{0,n_1,n_2}(k,\omega) - \sum_{\vec{k}'} \mathcal{P}^r_{0,n_1,n_2}(k,\omega) W\begin{pmatrix} n_1 n_2 n_1 n_2 \\ \vec{k}-\vec{k}' \end{pmatrix} \mathcal{P}^r_{n_1,n_2}(k',\omega), \tag{A13}$$

which gives rise directly to Eq. (36). A similar derivation yields

$$\mathcal{P}^<_{n_1,n_2}(k,\omega) = \mathcal{P}^<_{0,n_1,n_2}(k,\omega) - \sum_{\vec{k}'} W\begin{pmatrix} n_1 n_2 n_1 n_2 \\ \vec{k}-\vec{k}' \end{pmatrix} [\mathcal{P}^r_{0,n_1,n_2}(k,\omega)\mathcal{P}^<_{n_1,n_2}(k',\omega) + \mathcal{P}^<_{0,n_1,n_2}(k,\omega)\mathcal{P}^a_{n_1,n_2}(k',\omega)]. \tag{A14}$$

## APPENDIX B: THE MATRIX ELEMENTS OF THE SCREENED POTENTIAL

The eigenfunctions of the free-carrier Hamiltonian $H_0$ given by Eqs. (33a) and (33b) have slowly varying envelope and fast-varying atomiclike components. The latter are orthonormal and need not be considered here. The integrals can then be reduced to the envelope terms (envelope function approximation), and, for simplicity, we denote a given envelope function, $\phi_n(\vec{k},\vec{R}) \equiv 1/\sqrt{S}\,\exp(i\vec{k}\cdot\vec{R})F_n(\vec{k},z)$, where $S$ is the sample area. A general matrix element then has the form

$$\begin{aligned} W\begin{pmatrix} n_1 n_2 n_3 n_4 \\ \vec{q}_1 \vec{q}_2 \vec{q}_3 \vec{q}_4 \end{pmatrix} &= \int d\vec{R}_3 d\vec{R}_4 \phi^*_{n_1\vec{q}_1}(\vec{R}_3)\phi_{n_2\vec{q}_2}(\vec{R}_3) W(\vec{R}_3\vec{R}_4)\phi_{n_3\vec{q}_3}(\vec{R}_3)\phi^*_{n_4\vec{q}_4}(\vec{R}_4) \\ &= \frac{1}{S^2}\int d\vec{r}_3 d\vec{r}_4 e^{-i\vec{q}_1\cdot\vec{R}_3} e^{i\vec{q}_2\cdot\vec{R}_4} e^{i\vec{q}_3\cdot\vec{R}_3} e^{-i\vec{q}_4\cdot\vec{R}_4} \int dz_3 dz_4 F^*_{n_1}(\vec{q}_1,z_3)F_{n_2}(\vec{q}_2,z_4)F_{n_3}(\vec{q}_3,z_3) \\ &\quad \times F^*_{n_4}(\vec{q}_4,z_4) W(\vec{r}_3-\vec{r}_4;z_3-z_4) \\ &= \delta_{\vec{q}_1-\vec{q}_3,\vec{q}_2-\vec{q}_4} \int dz_3 dz_4 F^*_{n_1}(\vec{q}_1,z_3)F_{n_2}(\vec{q}_2,z_4)F_{n_3}(\vec{q}_1+\vec{\kappa},z_3)F^*_{n_4}(\vec{q}_4+\vec{\kappa},z_4)\int d\vec{\rho} e^{-i\vec{\rho}\cdot\vec{\kappa}} W(\vec{\rho},z_3,z_4) \\ &= \delta_{\vec{q}_1-\vec{q}_3,\vec{q}_2-\vec{q}_4} W\begin{pmatrix} n_1 n_2 n_3 n_4 \\ \vec{q}_1 \vec{q}_2 \vec{\kappa} \end{pmatrix}, \end{aligned} \tag{B1}$$

where $\vec{\kappa} = \vec{q}_1 - \vec{q}_3 = \vec{q}_2 - \vec{q}_4$. A concrete expression for the screened potential is necessary to go further. The general structure of the bare potential,

$$V(\vec{\rho},z,z') = \frac{e^2}{\epsilon_0}\sqrt{\rho^3 + (z-z')^2}, \tag{B2}$$

is readily obtained by using the expansion

$$\frac{1}{R} = \frac{2\pi}{S}\sum_{\vec{\xi}} \frac{1}{\xi} e^{i\vec{\xi}\cdot\vec{\rho}} e^{-\xi|z-z'|}, \tag{B3}$$

and can be expressed as

$$\begin{aligned} V\begin{pmatrix} n_1 n_2 n_3 n_4 \\ \vec{q}_1 \vec{q}_2 \vec{q}_3 \vec{q}_4 \end{pmatrix} &= \delta_{\vec{q}_1-\vec{q}_3,\vec{q}_2-\vec{q}_4} V\begin{pmatrix} n_1 n_2 n_3 n_4 \\ \vec{q}_1 \vec{q}_2 \vec{\kappa} \end{pmatrix} \\ &= \frac{2\pi e^2}{\epsilon_0 \kappa S} F\begin{pmatrix} n_1 n_2 n_3 n_4 \\ \vec{q}_1 \vec{q}_2 \vec{\kappa} \end{pmatrix}, \end{aligned} \tag{B4}$$

where the envelope-function form factor reads

$$\begin{aligned} F\begin{pmatrix} n_1 n_2 n_3 n_4 \\ \vec{q}_1 \vec{q}_2 \vec{\kappa} \end{pmatrix} &= \int dz_3 dz_4 F^*_{n_1}(\vec{q}_1,z_3)F_{n_2}(\vec{q}_2,z_4) \\ &\quad \times F_{n_3}(\vec{q}_1+\vec{\kappa},z_3)F^*_{n_4}(\vec{q}_4+\vec{\kappa},z_4) e^{-\kappa|z_3-z_4|}. \end{aligned} \tag{B5}$$

We then use the same general structure for the screened potential, leading to Eq. (A11).

## APPENDIX C: THE SCREENED LADDER APPROXIMATION FOR THE CARRIER SELF-ENERGY

We start the derivation by substituting the expression for the longitudinal vertex, Eq. (14a) into Eq. (12a) (transverse contributions are not considered). Next, we replace the remaining vertex by its first iteration, namely, $\gamma_{gf}(\underline{6}\ \underline{7}\ \underline{4}) \approx -\delta_{g,f}\delta(\underline{6}\ \underline{7})\delta(\underline{6}\ \underline{4})$, and obtain

$$\Sigma_{aa}(\underline{1}\ \underline{2}) = ie^2\hbar G_{aa}(\underline{1}\ \underline{2})W(\underline{2}\ \underline{1}) + e^2\hbar G_{aa}(\underline{1}\ \underline{3})W(\underline{6}\ \underline{1})t_{ad}(\underline{3}\ \underline{7}\ \underline{2}\ \underline{8}) \times G_{dd}(\underline{8}\ \underline{6})G_{dd}(\underline{6}\ \underline{7}), \tag{C1}$$

where we have introduced the quantity

$$t_{ab}(\underline{1}\ \underline{2}\ \underline{1'}\ \underline{2'}) = i\frac{\delta\Sigma_{aa}(\underline{1}\ \underline{1'})}{\delta G_{bb}(\underline{2'}\ \underline{2})}. \tag{C2}$$

Taking functional derivatives on both sides of Eq. (C2), we obtain a recurrence relation for $t_{ab}$. Bound-state contributions are obtained when $a \neq b$, with $a$ spanning the conduction and $b$ the valence bands (or vice versa). We outline here the derivation for $\{a,b\}=\{\text{conduction,valence}\}$, since the other case is analogous. We keep only the terms that yield a ladder approximation. In the other terms, we can replace $t_{ab}$ by its first order iteration. The resulting are higher order contributions that do not give rise to bound-state contributions and are thus neglected,[22]

$$t_{ab}(\underline{1}\ \underline{5}\ \underline{2}\ \underline{4}) = i\hbar^2e^4W(\underline{2}\ \underline{5})W(\underline{4}\ \underline{1})G_{aa}(\underline{1}\ \underline{2})G_{bb}(\underline{5}\ \underline{4}) + i\hbar e^2W(\underline{4}\ \underline{5})G_{aa}(\underline{1}\ \underline{3}) \times t_{ab}(\underline{3}\ \underline{5}\ \underline{2}\ \underline{8})G_{bb}(\underline{8}\ \underline{4}). \tag{C3}$$

Switching to the electron-hole picture, $\{a,b\}=\{e,h\}$, which leaves the conduction-band operators unaltered, but changes the valence-band operators (since the creation of a hole corresponds to the annihilation of a valence-band electron), and using $W_{eh}(\underline{1}\ \underline{2}) = -\hbar e^2 W(\underline{1}\ \underline{2})$, yields

$$t_{eh}(\underline{1}\ \underline{4}\ \underline{2}\ \underline{5}) = iW_{eh}(\underline{2}\ \underline{5})W_{eh}(\underline{4}\ \underline{1})G_{ee}(\underline{1}\ \underline{2})G_{hh}(\underline{4}\ \underline{5}) + iW_{eh}(\underline{4}\ \underline{1})G_{ee}(\underline{1}\ \underline{3}) \times t_{eh}(\underline{3}\ \underline{8}\ \underline{2}\ \underline{5})G_{hh}(\underline{4}\ \underline{8}). \tag{C4}$$

If we now define the $T$ matrix

$$t_{eh}(\underline{1}\ \underline{2}\ \underline{1'}\ \underline{2'}) = -\delta(\underline{1}\ \underline{1'})\delta(\underline{2}\ \underline{2'})W(\underline{1}\ \underline{2}) + T_{eh}(\underline{1}\ \underline{2}\ \underline{1'}\ \underline{2'}) \tag{C5}$$

and substitute Eq. (C5) into Eq. (C4), we obtain the $T$-matrix equation,

$$T_{eh}(\underline{1}\ \underline{2}\ \underline{1'}\ \underline{2'}) = \delta(\underline{1}\ \underline{1'})\delta(\underline{2}\ \underline{2'})W_{eh}(\underline{1}\ \underline{2}) + iW_{eh}(\underline{1}\ \underline{2})G_{ee}(\underline{1}\ \underline{3}) \times G_{hh}(\underline{2}\ \underline{4})T_{eh}(\underline{3}\ \underline{4}\ \underline{1'}\ \underline{2'}). \tag{C6}$$

The self-energy can then be written as a sum of a Hartree-Fock and a screened-ladder correlation contribution,

$$\Sigma_{ee}(\underline{1}\ \underline{1'}) = \Sigma^{\mathrm{HF}}_{ee}(\underline{1}\ \underline{1'}) + \Sigma^{c}_{ee}(\underline{1}\ \underline{1'}), \tag{C7a}$$

$$\Sigma^{\mathrm{HF}}_{ee}(\underline{1}\ \underline{1'}) = -i\hbar e^2 G(\underline{1}\ \underline{2})W(\underline{2}\ \underline{1}), \tag{C7b}$$

$$\Sigma^{c}_{ee}(\underline{1}\ \underline{1'}) = -iT''_{eh}(\underline{1}\ \underline{4}\ \underline{1'}\ \underline{5})G(\underline{5}\ \underline{4}), \tag{C7c}$$

where we have used Eq. (C6), and introduced the projected $T$ matrix, i.e., without the first two iterations,

$$T''_{eh}(\underline{1}\ \underline{2}\ \underline{1'}\ \underline{2'}) = T_{eh}(\underline{1}\ \underline{2}\ \underline{1'}\ \underline{2'}) - \delta(\underline{1}\ \underline{1'})\delta(\underline{2}\ \underline{2'})W_{eh}(\underline{1}\ \underline{2}) - iW_{eh}(\underline{1}\ \underline{2})W_{eh}(\underline{1'}\ \underline{2'}) \times G(\underline{1}\ \underline{1'})G(\underline{2}\ \underline{2'}). \tag{C8}$$

Note that $T_{eh}$ as defined by Eq. (C6) is the same $T$ matrix of Eq. (31) in terms of which the polarization function is written, which allows for a self-consistent computation of the self-energy and polarization functions in the same order in the Coulomb correlations.

## APPENDIX D: THE KMS RELATION FOR THE TRANSVERSE POLARIZATION FUNCTION

In order to prove that the transverse polarization function satisfies the Kubo-Martin-Schwinger (KMS) relation we start from an inspection of Eqs. (16a), (20), and (34). It is then clear that if $\mathcal{P}^{\lambda}_{n_1,n_2}(k,\omega)$ satisfies the KMS, then, automatically, $\mathcal{L}^{\lambda}_{n_1,n_2}(k,\omega)$ and $P^{\lambda}_{n_1,n_2}(k,\omega)$ also satisfy it.

Using the relation $2i\ \mathrm{Im}\{\mathcal{P}^{r}_{0,n_1,n_2}(k,\omega)\} = \mathcal{P}^{>}_{0,n_1,n_2}(k,\omega) - \mathcal{P}^{<}_{0,n_1,n_2}(k,\omega)$ and Eq. (37), we obtain

$$2\ \mathrm{Im}\{\mathcal{P}^{r}_{0,n_1,n_2}(k,\omega)\} = \hbar\int\frac{d\omega'}{2\pi}\hat{G}_{n_1n_1}(k,\omega')\hat{G}_{n_2n_2}(k,\omega-\omega')[1-f_e(\omega')-f_h(\omega-\omega')]$$

$$= \hbar[e^{\beta(\hbar\omega-\mu)}-1]\int\frac{d\omega'}{2\pi}\hat{G}_{n_1n_1}(k,\omega')\hat{G}_{n_2n_2}(k,\omega-\omega')f_e(\omega')f_h(\omega-\omega') \tag{D1a}$$

$$= i[1-e^{\beta(\hbar\omega-\mu)}]\mathcal{P}^{<}_{0,n_1,n_2}(k,\omega), \tag{D1b}$$

which is the KMS relation between $\mathcal{P}^{<}_{0,n_1,n_2}$ and Im $\mathcal{P}^{r}_{0,n_1,n_2}$. The next step is to inspect Eq. (A14) and use the fact that $\mathcal{P}^{<}_{0,n_1,n_2}(k,\omega)$ and $\mathcal{P}^{<}_{n_1,n_2}(k,\omega)$ are purely imaginary quantities, and $\mathcal{P}^{r}_{n_1,n_2}(k,\omega)=\mathcal{P}^{a}_{n_1,n_2}(k,\omega)^*$. Consequently,

$$\mathrm{Im}\{\mathcal{P}^{<}_{n_1,n_2}(k,\omega)\}\mathrm{Im}\{\mathcal{P}^{r}_{0,n_1,n_2}(k,\omega)\} - \mathrm{Im}\{\mathcal{P}^{<}_{0,n_1,n_2}(k,\omega)\}\mathrm{Im}\{\mathcal{P}^{r}_{n_1,n_2}(k,\omega)\}=0. \quad \text{(D2)}$$

Use of Eq. (D1b) gives rise to the KMS relation between $\mathrm{Im}\{\mathcal{P}^{<}_{n_1,n_2}(k,\omega)\}$ and $\mathcal{P}^{<}_{n_1,n_2}(k,\omega)$,

$$2\,\mathrm{Im}\{\mathcal{P}^{r}_{n_1,n_2}(k,\omega)\}=i[1-e^{\beta(\hbar\omega-\mu)}]\mathcal{P}^{<}_{n_1,n_2}(k,\omega). \quad \text{(D3)}$$

## APPENDIX E: SELF-CONSISTENT CALCULATION OF THE QUASICHEMICAL POTENTIALS

The average number of particles in a system of particles of type $a$ (electrons or holes) reads

$$N_a=\int \langle \Psi^{\dagger}_a(R)\Psi_a(R)\rangle dR, \quad \text{(E1)}$$

which can be expanded in the quantum-well basis defined by Eqs. (33a) and (33b),

$$N_a=\sum_{\substack{n_1 n_2\\ \vec{k}\vec{k}'}}\int \phi^*_{n_1\vec{k}}(R)\phi_{n_2\vec{k}'}(R)\langle\Psi^{\dagger}_{n_1\vec{k}}(R)\Psi_{n_2\vec{k}'}(R)\rangle dR$$

$$=-i\hbar\sum_{n_1\vec{k}}\int\frac{d\omega}{2\pi}G^{<}_{n_1n_1}(k,\omega)f_a(\omega)$$

$$=-i\hbar\sum_{n_1\vec{k}}\int\frac{d\omega}{2\pi}\hat{G}_{n_1n_1}(k,\omega)f_a(\omega) \quad \text{(E2a)}$$

$$=\sum_{n\vec{k}}\int\frac{d(\hbar\omega)}{2\pi}\frac{2\hbar\Gamma_n}{\hbar\omega-\hbar e_n(k)^2+\hbar^2\Gamma_n^2}f_a(\omega), \quad \text{(E2b)}$$

where we have the fact that the $\{\phi_n\}$ make an orthonormal basis. Equation (E2b) allows for the self-consistent computation of the chemical potentials including Coulomb correlations through the real and imaginary parts of the self-energy $\Sigma_{aa}$ included in $e_n(k)$ and $\Gamma_n(k)$. In the quasiparticle approximation, $\hbar\Gamma_n(k)\to 0$, we obtain the usual (spin summation is included in the subscript $n$)

$$N_a=\sum_{n\vec{k}} f_a(e_n(k)). \quad \text{(E3)}$$

## APPENDIX F: EFFICIENT NUMERICAL APPROXIMATION FOR THE RPA TRANSVERSE POLARIZATION FUNCTION

We have shown that, once $\mathcal{P}^{r}_{0,n_1,n_2}(k,\omega)$ satisfies the KMS relation, so does $\mathcal{P}^{r}_{n_1,n_2}(k,\omega)$. Here we present an approximation that allows for a fast computation of the RPA input, without the need for a numerical frequency integration of the spectral functions. We start from the exact Eq. (D1a), and note that the frequency-dependent inversion density can be expressed as

$$1-f_e(\omega')-f_h(\omega-\omega')=\{[1-f_e(\omega')][1-f_h(\omega-\omega')] + f_e(\omega')f_h(\omega-\omega')\} \times\tanh[(\beta\omega-\mu)/2]. \quad \text{(F1)}$$

The envelope term between curly brackets is then replaced by one, thus generalizing, for the full frequency-dependent case, an approximation for the inversion factor, actually included by hand in Ref. 24. By this procedure we demonstrate why the ansatz used in the past is accurate and give a step by step derivation for it. We further evaluate the dephasing factors at the peak of the corresponding spectral functions, and the frequency integration can be easily performed analytically,

$$\mathrm{Im}\ \mathcal{P}^{r}_{0,n_1,n_2}=\tanh[(\beta\omega-\mu)/2]\frac{-\Gamma_{n_1,n_2}}{\Gamma^2_{n_1,n_2}+(\omega-e_{n_1}-e_{n_2})^2}, \quad \text{(F2)}$$

where $\Gamma_{n_1,n_2}=\Gamma_{n_1}(e_{n_1})+\Gamma_{n_2}(e_{n_2})$, and Re $\mathcal{P}^{r}_{0,n_1,n_2}$ is computed by means of a Kramers-Kronig transformation. The KMS condition is fully satisfied by the expressions above, which can be used as a consistent and efficient input in the solution of the Bethe-Salpeter equation for the full polarization function.


[1] R. Zimmermann, *Many-Particle Theory of Highly Excited Semiconductors* (Teubner, Leipzig, 1987).

[2] S. Schmitt-Rink, C. Ell, and H. Haug, Phys. Rev. B **33**, 1183 (1986).

[3] M. Bayer, Ch. Schlier, Ch. Greus, A. Forchel, S. Benner, and H. Haug, Phys. Rev. B **55**, 13 180 (1997).

[4] M. F. Pereira, Jr., R. Binder, and S. W. Koch, Appl. Phys. Lett. **63**, 279 (1994).

[5] S. Bischoff, A. Knorr, and S. W. Koch, Phys. Rev. B **55**, 7715 (1997).

[6] L. P. Kadanoff and G. Baym, *Quantum Statistical Mechanics* (Benjamin, New York, 1962).

[7] M. F. Pereira, Jr. and K. Henneberger, Phys. Rev. B **53**, 16 485 (1996).

[8] K. Henneberger and H. Haug, Phys. Rev. B **38**, 9759 (1988).

[9] L. V. Keldysh, Zh. Éksp. Teor. Fiz. **20**, 4 (1965) [Sov. Phys. JETP **20**, 4 (1965)].

[10] K. Henneberger and S. W. Koch, Phys. Rev. Lett. **76**, 1820 (1996).

[11] M. F. Pereira, Jr., S. W. Koch, and W. W. Chow, J. Opt. Soc. Am. B **10**, 765 (1993).

[12] M. F. Pereira, Jr., R. Schepe, T. Schmielau, D. Tamme, and K. Henneberger (unpublished).

[13] R. Schepe, T. Schmielau, D. Tamme, and K. Henneberger, Phys.

Status Solidi B **206**, 273 (1998).
[14] M. Lindberg and S. W. Koch, Phys. Rev. B **38**, 3342 (1988).
[15] G. Bender, E. C. Larkins, H. Schneider, J. D. Ralston, and P. Koidl, Appl. Phys. Lett. **63**, 2920 (1993).
[16] Here we are discussing states bound in the quantum confinement (well) region, not states bound to impurities. For a textbook discussion, see G. Bastard, *Wave Mechanics of Semiconductor Heterostructures* (Les Editions de Physique, Les Ulis, 1989).
[17] I. V. Akimova and P. G. Eliseev, Proc. SPIE **2963**, 640 (1996).
[18] H. Grempel, A. Diessel, W. Ebeling, J. Gutowski, K. Schuell, B. Jobst, D. Hommel, M. F. Pereira, Jr., and K. Henneberger, Phys. Status Solidi B **194**, 199 (1996), and references therein.
[19] S. Hugues, A. Knorr, S. W. Koch, R. Binder, R. Indik, and J. Moloney, Solid State Commun. **100**, 555 (1996).
[20] C. H. Henry, R. A. Logan, and F. R. Merrit, J. Appl. Phys. **51**, 3042 (1980).
[21] A. Diessel, W. Ebeling, J. Gutowski, B. Jobst, K. Schuell, D. Hommel, and K. Henneberger, Phys. Rev. B **52**, 4736 (1995).
[22] P. Michler, M. Vehse, J. Gutowski, M. Behringer, D. Hommel, M. F. Pereira, Jr., and K. Henneberger, preceding paper, Phys. Rev. B **58**, 2055 (1998).
[23] For an alternative derivation with more detail in the case of electron-ion plasmas, see D. Tamme and K. Henneberger, Contrib. Plasma Phys. **37**, 265 (1997). A similar approximation has been used in the derivation that gives rise to the equations that have been numerically solved in Ref. 11 in the case of dense three-dimensional electron-hole plasmas.
[24] L. Banyai and S. W. Koch, Z. Phys. B **63l**, 283 (1986).